


## Magnon-Induced Nonreciprocity Based on the Magnon Kerr Effect

Cui Kong,<sup>\*</sup> Hao Xiong,<sup>†</sup> and Ying Wu<sup>‡</sup>

*School of Physics, Huazhong University of Science and Technology, Wuhan 430074, People's Republic of China*

 (Received 6 June 2019; revised manuscript received 5 August 2019; published 3 September 2019)

Nonreciprocal devices that allow unidirectional wave propagation are indispensable in many scientific fields, including, for example, optics, acoustics, electronics, and thermodynamics. Here, we propose to realize the nonreciprocal transmission of a microwave field in a two-cavity magnonics system consisting of two microwave cavities and a yttrium iron garnet (YIG) sphere, which is placed in one of them. We discover that magnon Kerr nonlinearity leads to the occurrence of magnon bistability and different magnonic responses for the forward and backward propagation of a microwave field. The different magnonic responses play a crucial role in the nonreciprocal transmission, which essentially breaks the space-reversal symmetry of transmission of the microwave field. More importantly, by adjusting the external bias magnetic field, which determines the frequency of the magnon, we can obtain a variable isolation of the microwave field or even its transmission in only one direction, which may be utilized to achieve light diodes. In addition, by increasing the strength of a microwave source applied to drive the magnon mode, stronger nonreciprocal transmission can be observed. These results may open a route to exploiting various nonreciprocal effects in cavity magnonics systems.

DOI: [10.1103/PhysRevApplied.12.034001](https://doi.org/10.1103/PhysRevApplied.12.034001)

### I. INTRODUCTION

Recently, the cavity magnonics system has drawn considerable attention in physics, due to the strong or even ultrastrong couplings of collective spin excitations in a millimeter-scale yttrium iron garnet (YIG) crystal and the cavity photons [1–6]. Especially for the YIG sphere [7–10], it possesses a low damping rate [11], which is a challenging task for spin ensembles in paramagnetic materials [12–14] and a high spin density in contrast to spin ensembles in dilute paramagnetic systems, e.g., nitrogen-vacancy centers in diamond [15]. Benefiting from the advantages of the magnons, this hybrid system is also expected to become a building block of the future quantum-information network. Besides the coupling of the magnons to the microwave-cavity photons, the couplings between the magnons and other quantum systems, including the superconducting qubit [16,17], phonons [18], and optical whispering-gallery modes [19–21], have been demonstrated. Furthermore, due to the merits of a long coherence time [10] and intrinsically good tunability compared to a variety of cavity electro- and optomechanical systems [22], the cavity magnonics system has become a promising platform for the implementation of various exotic phenomena, such as magnon-induced transparency [23], non-Hermitian physics [24–26], magnon

dark modes in a magnon-gradient memory [27], the emerging field of spintronics [28–30], and cooperative polariton dynamics [31].

In addition to the cavity magnon-polaritons as quasiparticles originating from the strong coupling of magnons to cavity photons, it is worth mentioning that the concept of the magnon Kerr effect, which results from the magnetocrystalline anisotropy in the YIG crystal, has been put forward in a strongly coupled cavity-magnon system and has also been experimentally demonstrated [32,33]. Due to magnon Kerr nonlinearity, which is beyond the conventional linearized description of a general cavity magnonics system [25], it brings about some fascinating phenomena, such as the bistability of cavity magnon-polaritons [34] and magnon-induced high-order sideband generation [35]. In parallel, the properties and applications of the nonreciprocity induced by the nonlinearity have attracted intense interest in recent years [36–43]. In order to realize nonreciprocity, the time-reversal symmetry inherent in the governing electromagnetic wave equations in linear and nonmagnetic media needs to be broken [44]. Traditionally, there is an avenue to break the time-reversal symmetry based on the magneto-optical (Faraday-rotation) crystals [45,46], which has the disadvantage of being bulky, costly, and unsuitable for on-chip integration. With rapidly growing interest in optomechanical systems as a class of microscale integrable devices, nonreciprocal devices including isolators, circulators, and directional amplifiers have been proposed theoretically [47] and realized experimentally [48,49]. Inspired by the conversion between

<sup>\*</sup>cuihong@hust.edu.cn

<sup>†</sup>haoxiong1217@gmail.com

<sup>‡</sup>yingwu2@126.com

microwave and optical fields via electro-optomechanical systems, we propose a scheme for achieving the nonreciprocity of a microwave field in a two-cavity magnonics system, which has great flexibility in contrast to optomechanical systems, since the frequency of the magnons can be tuned at will by adjusting the bias magnetic field [50,51]. However, despite its emergence as the fundamental principle of isolators and circulators, which are very important devices for information processing [52–54], the nonreciprocal effect is still unexplored in cavity magnonics systems.

In the present work, we put forward a two-cavity magnonics system comprised of two microwave cavities and a YIG sphere to achieve the nonreciprocal transmission of a microwave field, where the Lorentz reciprocity is broken on the basis of magnon Kerr nonlinearity. We observe the bistability of magnons and different magnonic responses where, in particular, the magnonic response plays a vital role in the study of the transmission of the microwave field and different magnonic responses make the implementation of the nonreciprocal transmission possible. There are two cases for the realization of the nonreciprocity, relying on either the destruction of the impedance-matching condition [55], for which the different magnonic responses need to be strong enough, or by directly driving the magnon mode with a microwave source, even if the impedance-matching condition is satisfied. In addition, taking advantage of the great flexibility of adjustment of the frequency of the magnon, a variable isolation of the transmission of a microwave field can be seen, which is easy to operate in practice. Moreover, by increasing the strength of the driving field on the magnon mode, the nonreciprocal isolation rate gets further improved and even an extremely high forward-to-backward-incidence extinction ratio ( $> 20$  dB) [56] can be reached, due to the magnon Kerr nonlinearity having a more marked effect. These results may deepen our understanding of magnon Kerr nonlinearity and open a door toward the synthesis of novel microscale magnon structures for potential applications in isolators, on-chip light control, and optical communications.

The paper is organized as follows. In Sec. II, we introduce the theoretical mode and show the bistability of the magnon numbers based on magnon Kerr nonlinearity. In Sec. III, we discuss the nonreciprocal transmission of a microwave field. In Sec. IV, we conclude by summarizing the results.

## II. THEORETICAL MODEL AND DERIVATION OF MAGNON BISTABILITY IN A TWO-CAVITY MAGNONICS SYSTEM

As shown in Fig. 1(a), the proposed two-cavity magnonics system consists of two microwave cavities and a YIG sphere, where the YIG sphere is placed in the right cavity.

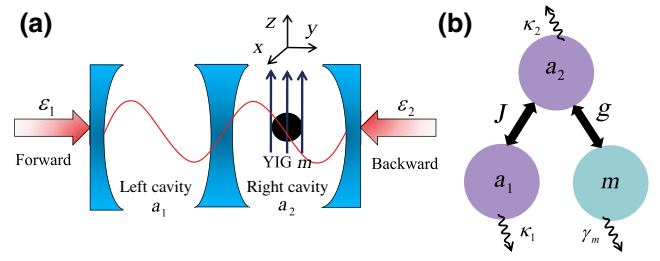


FIG. 1. (a) A schematic diagram of a two-cavity magnonics system, consisting of two microwave cavities and a YIG sphere, which is placed in the right cavity. (b) A schematic diagram of the linear coupling of the right-cavity photon to the left-cavity photon and the magnon, with the coupling strengths  $J$  and  $g$ , respectively.  $\kappa_1$ ,  $\kappa_2$ , and  $\gamma_m$  are the dissipation rates of the two cavities and the magnon mode, respectively.

A uniform external magnetic field ( $H$ ) is applied along the  $z$  direction to bias the YIG sphere. The two cavities are diametrically driven by the microwave fields with the driving strengths  $\varepsilon_1$  and  $\varepsilon_2$ , respectively; the magnon mode is also directly driven by a microwave source (not shown). In Fig. 1(b), the interconnects between the two cavity photons can be created using superconducting transmission lines [57] on the one hand, while, on the other, the photons of the right cavity couple to the magnons in the YIG sphere via the collective magnetic-dipole interaction. When all of the driving fields are included, the total Hamiltonian of the system can be written (for  $\hbar = 1$ ) as follows [33,34]:

$$\begin{aligned} \hat{H} = & \omega_1 \hat{a}_1^\dagger \hat{a}_1 + \omega_2 \hat{a}_2^\dagger \hat{a}_2 + \omega_m \hat{m}^\dagger \hat{m} + K \hat{m}^\dagger \hat{m} \hat{m}^\dagger \hat{m} \\ & + J (\hat{a}_1^\dagger \hat{a}_2 + \hat{a}_1 \hat{a}_2^\dagger) + g (\hat{a}_2^\dagger \hat{m} + \hat{a}_2 \hat{m}^\dagger) \\ & + i\sqrt{\eta_1 \kappa_1} \varepsilon_1 (\hat{a}_1^\dagger e^{-i\omega_d t} - \hat{a}_1 e^{i\omega_d t}) \\ & + i\sqrt{\eta_2 \kappa_2} \varepsilon_2 (\hat{a}_2^\dagger e^{-i\omega_d t} - \hat{a}_2 e^{i\omega_d t}) \\ & + i\sqrt{\eta_3 \gamma_m} \varepsilon_3 (\hat{m}^\dagger e^{-i\omega_d t} - \hat{m} e^{i\omega_d t}). \end{aligned} \quad (1)$$

Here,  $\hat{a}_i$  ( $\hat{a}_i^\dagger$ ) is the annihilation (creation) operator of the cavity mode ( $i = 1, 2$ ) with resonance frequency  $\omega_i$ . The boson operator  $\hat{m}$  is the magnon mode at frequency  $\omega_m$ , determined by the external bias magnetic field  $H$  via  $\omega_m = \gamma H$ , where  $\gamma/2\pi = 28$  GHz/T is the gyromagnetic ratio. The term  $K \hat{m}^\dagger \hat{m} \hat{m}^\dagger \hat{m}$  denotes the Kerr effect of magnons due to the magnetocrystalline anisotropy in the YIG sphere, where  $K = \mu_0 K_{\text{an}} \gamma / (M^2 V_m)$  is the Kerr nonlinear coefficient, in which  $\mu_0$  is the magnetic permeability of free space,  $K_{\text{an}}$  is the first-order anisotropy constant,  $\gamma$  is the gyromagnetic ratio,  $M$  is the saturation magnetization, and  $V_m$  is the volume of the YIG sphere.  $J$  is the photon coupling rate and  $g$  is the linear photon-magnon coupling strength, which can be adjusted by varying the direction of the bias field or the position of the YIG sphere

inside the right cavity [18]. The rest describes the couplings of the driving fields to the two microwave cavities and the magnons, the amplitudes of the driving fields being  $\varepsilon_j = \sqrt{P_j/\hbar\omega_d}$  ( $j = 1, 2, 3$ ) where the corresponding input power and frequency are  $P_j$  and  $\omega_d$ , respectively.  $\kappa_i$  represents the total loss rate of the cavity mode, which contains an intrinsic loss rate  $\kappa_{i,0}$  and an external loss rate  $\kappa_{i,e}$  [22].  $\gamma_m$  is the total loss rate of the magnon mode. The coupling parameter  $\eta_i = \kappa_{i,e}/\kappa_i$ , which describes the coupling between the driving field and the cavity mode, can be continuously adjusted [22]. Analogously,  $\eta_3$  is the magnon coupling parameter.

In the semiclassical limit, the operators can be reduced to their expectation values, viz.,  $\langle \hat{a}_1 \rangle = a_1$ ,  $\langle \hat{a}_2 \rangle = a_2$ , and  $\langle \hat{m} \rangle = m$ , and the quantum-noise terms can safely be dropped because their expectation values are zero. In the rotating frame of the driving frequency  $\omega_d$ , the evolution of the two-cavity magnonics system can be described by the Heisenberg-Langevin equations as follows:

$$\dot{a}_1 = (-i\Delta_1 - \kappa_1/2)a_1 - iJA_2 + \sqrt{\eta_1\kappa_1}\varepsilon_1, \quad (2)$$

$$\dot{a}_2 = (-i\Delta_2 - \kappa_2/2)a_2 - iJA_1 - igm + \sqrt{\eta_2\kappa_2}\varepsilon_2, \quad (3)$$

$$\dot{m} = (-i\Delta_m - \gamma_m/2)m - igA_2 - i(2Km^*m + K)m + \sqrt{\eta_3\gamma_m}\varepsilon_3, \quad (4)$$

in which the detuning parameters are  $\Delta_1 = \omega_1 - \omega_d$ ,  $\Delta_2 = \omega_2 - \omega_d$ , and  $\Delta_m = \omega_m - \omega_d$ .

In order to solve the nonlinear Eqs. (2)–(4), the operators of the photon and magnon modes can be rewritten as a sum of the steady-state value and the fluctuation, i.e.,  $a_1 = A_1 + \delta a_1$ ,  $a_2 = A_2 + \delta a_2$ , and  $m = M + \delta m$ . It follows from Eqs. (2)–(4) that  $A_1$ ,  $A_2$ , and  $M$  satisfy the following:

$$0 = (-i\Delta_1 - \kappa_1/2)A_1 - iJA_2 + \sqrt{\eta_1\kappa_1}\varepsilon_1, \quad (5)$$

$$0 = (-i\Delta_2 - \kappa_2/2)A_2 - iJA_1 - igM + \sqrt{\eta_2\kappa_2}\varepsilon_2, \quad (6)$$

$$0 = (-i\Delta_m - \gamma_m/2)M - igA_2 - i(2K|M|^2 + K)M + \sqrt{\eta_3\gamma_m}\varepsilon_3. \quad (7)$$

In the present work, we are interested in the mean response of the system to the driving-field input on the cavity. In order to study the transmission of the microwave field in the forward and backward directions of the driving-field input, we let  $\varepsilon_1 \neq 0$  and  $\varepsilon_2 = 0$ , representing the driving-field input from the left cavity, and  $\varepsilon_2 \neq 0$  and  $\varepsilon_1 = 0$ , representing the driving-field input from the right cavity.

When we set  $\varepsilon_1 \neq 0$  and  $\varepsilon_2 = 0$ , the steady-state solution of Eqs. (5)–(7) can be obtained as follows:

$$A_1 = \frac{\sqrt{\eta_1\kappa_1}\varepsilon_1 - iJA_2}{i\Delta_1 + \kappa_1/2}, \quad (8)$$

$$A_2 = \frac{-iJ\sqrt{\eta_1\kappa_1}\varepsilon_1 + gM(\Delta_1 - i\kappa_1/2)}{(i\Delta_1 + \kappa_1/2)(i\Delta_2 + \kappa_2/2) + J^2}, \quad (9)$$

$$M = \left[ \sqrt{\eta_3\gamma_m}\varepsilon_3 - \frac{gJ\sqrt{\eta_1\kappa_1}\varepsilon_1}{(i\Delta_1 + \kappa_1/2)(i\Delta_2 + \kappa_2/2) + J^2} \right] / \Upsilon, \quad (10)$$

where

$$\Upsilon = i(\Delta_m + 2K|M|^2 + K) + \gamma_m/2 + \frac{g^2(i\Delta_1 + \kappa_1/2)}{(i\Delta_1 + \kappa_1/2)(i\Delta_2 + \kappa_2/2) + J^2}. \quad (11)$$

According to Eq. (10), we have a third-order nonlinear equation for the magnon number  $M_{10} = |M|^2$ ,

$$t_3 |M_{10}|^3 + t_2 |M_{10}|^2 + t_1 M_{10} - d_1 = 0, \quad (12)$$

with

$$t_3 = 4K^2, \quad (13)$$

$$t_2 = 4K\alpha + \frac{4K\zeta(\gamma_m\beta/2 + g^2\Delta_1) - 4K\beta(\gamma_m\zeta/2 + g^2\kappa_1/2)}{\beta^2 + \zeta^2}, \quad (14)$$

$$t_1 = \alpha^2 + \frac{(\gamma_m\zeta/2 + g^2\kappa_1/2)^2 + (\gamma_m\beta/2 + g^2\Delta_1)^2}{\beta^2 + \zeta^2} + \frac{2\alpha\zeta(\gamma_m\beta/2 + g^2\Delta_1) - 2\alpha\beta(\gamma_m\zeta/2 + g^2\kappa_1/2)}{\beta^2 + \zeta^2}, \quad (15)$$

and

$$d_1 = \frac{\eta_3\gamma_m\varepsilon_3^2\beta^2 + (\sqrt{\eta_3\gamma_m}\varepsilon_3\zeta - gJ\sqrt{\eta_1\kappa_1}\varepsilon_1)^2}{\beta^2 + \zeta^2}, \quad (16)$$

in which  $\alpha = \Delta_m + K$ ,  $\beta = \Delta_1\kappa_2/2 + \Delta_2\kappa_1/2$ , and  $\zeta = \kappa_1\kappa_2/4 + J^2 - \Delta_1\Delta_2$ .

When we set  $\varepsilon_2 \neq 0$  and  $\varepsilon_1 = 0$ , the steady-state solutions of Eqs. (5)–(7) are rewritten as follows:

$$A_1 = \frac{-iJA_2}{i\Delta_1 + \kappa_1/2}, \quad (17)$$

$$A_2 = \frac{(\sqrt{\eta_2\kappa_2}\varepsilon_2 - igM)(i\Delta_1 + \kappa_1/2)}{(i\Delta_1 + \kappa_1/2)(i\Delta_2 + \kappa_2/2) + J^2}, \quad (18)$$

$$M = \left[ \sqrt{\eta_3\gamma_m}\varepsilon_3 - \frac{(igJ\sqrt{\eta_2\kappa_2}\varepsilon_2)(i\Delta_1 + \kappa_1/2)}{(i\Delta_1 + \kappa_1/2)(i\Delta_2 + \kappa_2/2) + J^2} \right] / \Upsilon. \quad (19)$$

From Eq. (19), we also obtain a third-order nonlinear equation for the magnon number  $M_{20} = |M|^2$ ,

$$t_3 |M_{20}|^3 + t_2 |M_{20}|^2 + t_1 M_{20} - d_2 = 0, \quad (20)$$

with

$$d_2 = \frac{(\sqrt{\eta_3\gamma_m}\varepsilon_3\beta - g\sqrt{\eta_2\kappa_2}\varepsilon_2\kappa_1/2)^2}{\beta^2 + \zeta^2} + \frac{(\sqrt{\eta_3\gamma_m}\varepsilon_3\zeta + g\sqrt{\eta_2\kappa_2}\varepsilon_2\Delta_1)^2}{\beta^2 + \zeta^2}. \quad (21)$$

Before demonstrating the nonreciprocal transmission of a microwave field in the two-cavity magnonics system, which lies at the core of this paper, we give the magnonic response (the magnon number of the steady state) to the forward or backward driving-field input. Comparing Eq. (12) with Eq. (20), it is found that the only difference is the zero-order term of the third-order nonlinear equation for the magnon number, which illustrates that the steady state of the two-cavity magnonics system changes when the direction of the driving-field input is reversed. However, the same magnonic response may be obtained for the driving-field input from different cavity modes, when some conditions are satisfied. In a case in which no microwave source is driving the magnon mode, we find that when

$$\eta_1\kappa_1J^2 = \eta_2\kappa_2(\Delta_1^2 + \kappa_1^2/4), \quad (22)$$

the same magnonic response is observed for the different directions (forward or backward incidence) of the driving-field input. We regard Eq. (22) as an impedance-matching condition [55] for the same magnonic response. Conversely, if the impedance-matching condition is broken, different magnonic responses occur. In another case of a microwave source driving the magnon mode, even if the impedance-matching condition is satisfied, different magnonic responses may emerge. Therefore, there are two cases that need to be considered to achieve different magnonic responses, including the destruction of the impedance-matching condition and a microwave source driving the magnon mode, which play a key role in the discussion of the nonreciprocal transmission of a microwave field.

In Fig. 2, the steady-state magnon numbers are plotted as a function of the input power  $P_{\text{in}}$  ( $P_1$ ,  $P_2$  and  $P_3$ ), where the magnon numbers  $M_{10}$  and  $M_{20}$  correspond to the driving field injected in the forward and backward cavity directions. These figures show a bistable behavior of the magnon numbers in the two-cavity magnonics system, which is very similar to a cavity magnonics system consisting of single-cavity photons strongly interacting with the magnons in a small YIG sphere [34]. Especially for Fig. 2(a), we show the generation of the magnon numbers by only driving the magnon mode. In comparison with a cavity in Ref. [34], we find that, close to the experimental parameter in a cavity, the drive power required to observe the bistability of magnon numbers in our two cavities is about 100 mW.

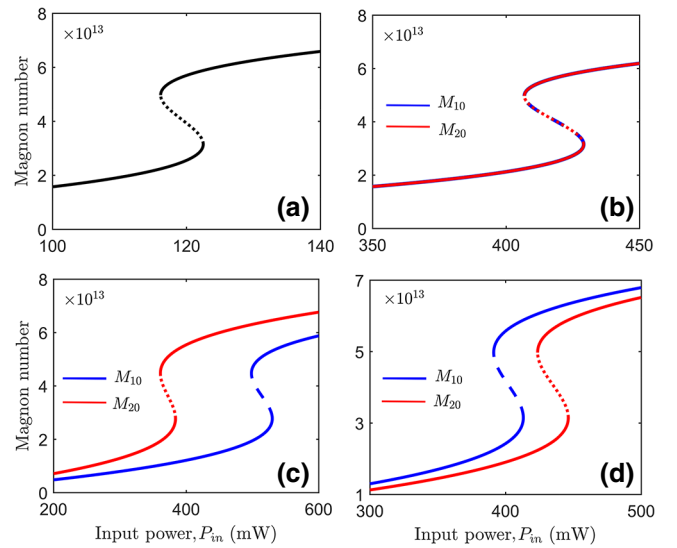


FIG. 2. The steady-state magnon number plotted as a function of the input power  $P_{\text{in}}$ , including  $P_1$ ,  $P_2$ , and  $P_3$ : (a)  $P_1 = P_2 = 0$  and  $J = 0.5874\gamma_m$  ( $J = \sqrt{(\Delta_1^2 + \kappa_1^2/4)/3}$ ); (b)  $P_3 = 0$  and  $J = 0.5874\gamma_m$ ; (c)  $P_3 = 0$  and  $J = 0.5\gamma_m$ ; (d)  $P_3 = 50 \mu\text{W}$  and  $J = 0.5874\gamma_m$ . The other parameters are  $\omega_m/2\pi = 10.1 \text{ GHz}$ ,  $\kappa_2/2\pi = 5 \text{ MHz}$ ,  $\kappa_1 = 3\kappa_2$ ,  $\gamma_m/2\pi = 40 \text{ MHz}$ ,  $g/2\pi = 41 \text{ MHz}$ ,  $K/2\pi = 5 \times 10^{-7} \text{ Hz}$ ,  $\eta_1 = \eta_2 = \eta_3 = 0.5$ ,  $\Delta_m = 0$ , and  $\Delta_1 = \Delta_2 = \gamma_m$ , which are mostly based on the latest experimental parameters [32,34].

However, we take no account of a driving field coupled to the magnon mode and mainly concentrate on the steady-state magnon numbers varying with the driving field applied on the microwave cavities in the forward and backward directions. As shown in Fig. 2(b), when the impedance-matching condition given by Eq. (22) is satisfied, the magnonic responses are the same and the dependent-variable magnon numbers  $M_{10}$  and  $M_{20}$  change synchronously. In addition, it can be seen that the drive power required to observe the bistability of magnon numbers is larger than its counterpart in Fig. 2(a), which involves the influence of other parameters, such as the coupling strength between the two cavities, and the corresponding conclusions can be drawn from Eqs. (16) and (21). Once the impedance-matching condition is broken in Fig. 2(c), the magnonic responses are no longer the same due to the appearance of two distinct bistable curves; for instance, the related isolation of the magnon numbers is about 2.1 dB for the input power  $P_{\text{in}} = 300 \text{ mW}$  and the coupling strength between the two cavities is  $J = 0.5\gamma_m$ . Besides the destruction of the impedance-matching condition as one approach to constructing two different magnonic responses, an additional microwave source, which is used to drive the magnon mode directly, can also produce different magnonic responses for the driving field transmitting in the forward or backward directions,

as shown in Fig. 2(d). Owing to the different magnonic responses, nonreciprocal transmission of the microwave-field behavior in the proposed two-cavity magnonics structure may emerge, which brings about some applications, such as isolators or light diodes. In contrast to linear isolators that are independent of the strength of the driving-field input, here we instead break the Lorentz reciprocity by using magnon Kerr nonlinearity, which relies on the input drive power.

### III. DISCUSSION OF THE NONRECIPROCAL TRANSMISSION OF A MICROWAVE FIELD

In what follows, we mainly discuss the effects of the parameters on the nonreciprocal transmission of a microwave field with a forward and backward driving-field input by solving the equations numerically. Substituting Eqs. (9) and (17) into the standard input-output relation [58], the output fields  $A_{2,\text{out}}$  and  $A_{1,\text{out}}$  can be written as follows:

$$A_{2,\text{out}} = \sqrt{\eta_2 \kappa_2} A_2 = \frac{-iJ \sqrt{\eta_1 \kappa_1 \eta_2 \kappa_2} \varepsilon_1 + \sqrt{\eta_2 \kappa_2} g M (\Delta_1 - i\kappa_1/2)}{(i\Delta_1 + \kappa_1/2)(i\Delta_2 + \kappa_2/2) + J^2}, \quad (23)$$

$$A_{1,\text{out}} = \sqrt{\eta_1 \kappa_1} A_1 = \frac{-iJ \sqrt{\eta_1 \kappa_1 \eta_2 \kappa_2} \varepsilon_2 - \sqrt{\eta_1 \kappa_1} g J M}{(i\Delta_1 + \kappa_1/2)(i\Delta_2 + \kappa_2/2) + J^2}. \quad (24)$$

In addition, we define  $T_{21}$  and  $T_{12}$  as the transmission coefficients for the driving-field input from the forward and backward directions, with

$$T_{21} \equiv \left| \frac{A_{2,\text{out}}}{\varepsilon_1} \right|, \quad T_{12} \equiv \left| \frac{A_{1,\text{out}}}{\varepsilon_2} \right|, \quad (25)$$

where the output fields  $|A_{2,\text{out}}|^2$  and  $|A_{1,\text{out}}|^2$  are dependent on the magnonic response of the system steady state and thus rely on the direction of the driving-field incidence.

In the absence of any consideration of a microwave source driving the magnon mode, we show the magnon numbers and the transmission coefficients for different two-cavity coupling strengths  $J$  and drive powers ( $P_1$  and  $P_2$ ) as a function of the detuning  $\Delta_1/\gamma_m$  in Fig. 3. When the impedance-matching condition ( $J = \sqrt{(\Delta_1^2 + \kappa_1^2/4)/3}$ ) is established in Figs. 3(a) and 3(b), not only are the same magnon numbers obtained—that is,  $M_{10} = M_{20}$ —but also reciprocal transmission can be observed due to  $T_{21} = T_{12}$ , which verifies the correctness of the same-magnonic-response effect. Furthermore, one can see two transmission windows of the microwave field, resulting from the coherent conversion among the two microwave cavity photons and

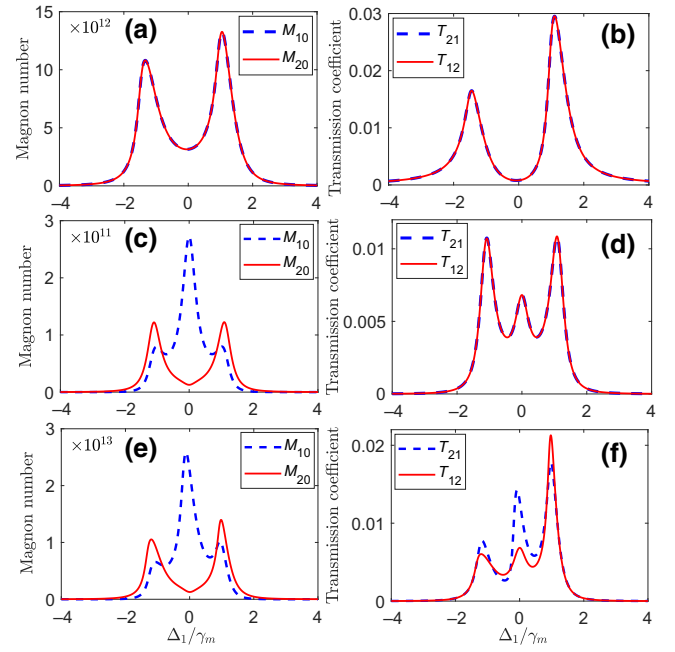


FIG. 3. The magnon numbers  $M_{10}$  (blue) and  $M_{20}$  (red) and the transmission coefficients  $T_{21}$  (blue) and  $T_{12}$  (red) as a function of the detuning  $\Delta_1/\gamma_m$ : (a),(b)  $J = \sqrt{(\Delta_1^2 + \kappa_1^2/4)/3}$  and  $P_1 = P_2 = 100$  mW; (c),(d)  $J = 0.5\gamma_m$  and  $P_1 = P_2 = 1$  mW; (e),(f)  $J = 0.5\gamma_m$  and  $P_1 = P_2 = 100$  mW.  $P_3 = 0$  mW,  $\Delta_m = \Delta_2 = \Delta_1$ , and the other parameters are the same as in Fig. 2.

the magnons. Once the impedance-matching condition is broken, as shown in Figs. 3(c) and 3(d), two kinds of magnon-number distributions are presented in Fig. 3(c), but we still cannot observe nonreciprocal transmission with a weak drive power (1 mW) in Fig. 3(d), where the effective magnon Kerr nonlinearity does not break the spatial symmetry of the transmission of the microwave field. For comparison, the identical two-cavity coupling strength  $J = 0.5\gamma_m$  is given, but the drive power is increased to 100 mW in Figs. 3(e) and 3(f). We observe three transparency windows with the amplitudes of  $T_{21}$  distinct from those of  $T_{12}$ , which is indicative of magnon-induced nonreciprocity via different and strong magnonic responses.

To obtain a more comprehensive analysis of the nonreciprocal transmission of a microwave field, we plot the magnon numbers and the transmission coefficients with respect to the external magnetic field  $H$ , which determines the frequency of the magnon. Except for the destruction of the impedance-matching condition, which leads to nonreciprocal transmission, here we show another case in which nonreciprocal transmission of a microwave field can be achieved, by using a microwave source to drive the magnon mode. For one case in which the impedance-matching condition is broken with  $J = 0.5\gamma_m$ , shown in Figs. 4(a) and 4(b), the large amplitude differences of

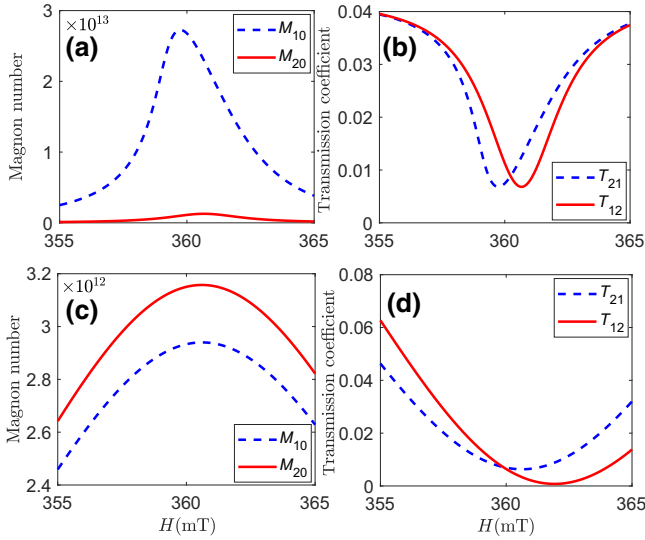


FIG. 4. The magnon numbers  $M_{10}$  (blue) and  $M_{20}$  (red) and the transmission coefficients  $T_{21}$  (blue) and  $T_{12}$  (red) as a function of the external magnetic field  $H$ : (a),(b)  $J = 0.5\gamma_m$  and  $P_3 = 0$  mW; (c),(d)  $J = \sqrt{(\Delta_1^2 + \kappa_1^2)/4}/3$  and  $P_3 = 10$  mW.  $P_1 = P_2 = 100$  mW,  $\Delta_2 = \Delta_1 = 0$ , and the other parameters are the same as in Fig. 2.

two magnon numbers are distributed around  $H = 360$  mT, with the magnetic field away from  $H = 360$  mT, and the amplitude differences of two magnon numbers decrease gradually in Fig. 4(a). We now turn to observing the transmission coefficients of a microwave field from the forward and backward directions in Fig. 4(b). It is found that the nonreciprocal transmission can be reflected in a small range at  $H \in (358, 362)$  mT, which is also the corresponding region of the profoundly different magnon responses. In the other case, under the condition  $J = \sqrt{(\Delta_1^2 + \kappa_1^2)/4}/3$ , which meets the impedance-matching condition, the magnon mode is driven by a microwave source with  $P_3 = 10$  mW, as shown in Figs. 4(c) and 4(d). We can intuitively see two almost equidistant arc curves in Fig. 4(c). Compared to Fig. 4(a), the adjustability of the magnetic field is not pronounced enough to obtain large-amplitude differences of two magnon numbers. Nevertheless, from the perspective of the nonreciprocal transmission of a microwave field,  $T_{21}$  is always different from  $T_{12}$  in Fig. 4(d), which amply demonstrates the controllability of the magnetic field upon nonreciprocal transmission. It is worth emphasizing that all parameters selected in the transmission of the microwave field are independent of its bistability.

The efficiency of the nonreciprocal transmission of a microwave field can be described by the isolation, as follows:

$$I = 10 \left| \log_{10} \frac{|A_{2,\text{out}}|^2}{|A_{1,\text{out}}|^2} \right|, \quad (26)$$

given in decibels. For the case of reciprocal transmission, we have  $|A_{2,\text{out}}|^2 / |A_{1,\text{out}}|^2 = 1$  and  $I = 0$ . A nonzero  $I$  presents nonreciprocal transmission and the greater the value of  $I$ , the higher is the degree of the nonreciprocal transmission.

The calculation results for  $I$ , plotted as a function of the detuning  $\Delta_1/\gamma_m$  and the external magnetic field  $H$ , are shown in Fig. 5, which gives us a clearer perspective for the differences between the transmission coefficients  $T_{21}$  and  $T_{12}$ . With the frequency of the driving field or that of  $H$  varying, we implement a variable light isolation and obtain a higher nonreciprocal isolation ratio in Fig. 5(b). Comparing Fig. 5(a) with Fig. 5(b), two distinct structural styles appear, that one bright area is a cross and other bright area is two columns. As shown in Fig. 5(a), the bright regions are mainly centralized near the central symmetry point at  $H = 353$  mT and  $\Delta_1/\gamma_m = 0$ , where the maximal value of  $I$  is only 8.05 dB. However, in Fig. 5(b), the bright regions are concentrated in the range of  $\Delta_1/\gamma_m > 0$  and  $H \in (350, 357.5)$  mT, with the maximal value of  $I$  far exceeding 8.05 dB and reaching 17.2 dB, which categorically reaches a higher nonreciprocal isolation ratio, and this may be used to achieve light diodes. These values indicate that the destruction of the impedance-matching condition and a microwave source driving the magnon mode have different effects on the nonreciprocal transmission of a microwave field, but both allow us to obtain a variable nonreciprocal isolation, by adjusting the external magnetic field  $H$  originating from different magnonic responses, in contrast to previous studies [42,43,55]. In addition, it is noteworthy that in Fig. 5(a), the input power  $P_1 = P_2 = 200$  mW, while in Fig. 5(b) the input power is equal to 100 mW, which is half the value compared to in Fig. 5(a). This illustrates that a better result is exhibited by making the effective magnon Kerr nonlinearity improve by directly driving the magnon mode and, further, that different magnonic responses bring about nonreciprocal transmission via the breaking of the spatial symmetry of the transmission of the microwave field.

To obtain robust nonreciprocal isolation, we show the efficiency  $I$  for the nonreciprocal transmission of a microwave field as a function of the detuning  $\Delta_1/\gamma_m$  for different input powers  $P_3$  in Fig. 6, where we combine two cases of obtaining the nonreciprocal transmission, with the other parameters given as  $J = 0.5\gamma_m$ ,  $P_1 = P_2 = 100$  mW, and  $\Delta_m = \Delta_2 = \Delta_1$ . When the input power of the driving field  $P_3 = 0$  W and the impedance-matching condition is broken due to  $J = 0.5\gamma_m$ , the magenta curve shows a nonreciprocal transmission effect in the range of  $\Delta_1/\gamma_m \in (-1.3, 1.2)$ , which agrees with the conclusion from Figs. 3(e) and 3(f). However, without the driving on the magnon mode, the effective magnon Kerr nonlinearity is too weak to produce a strong nonreciprocal transmission effect. As shown by the blue dotted curve, where  $P_3 = 1$  mW, the parameter range of the detuning

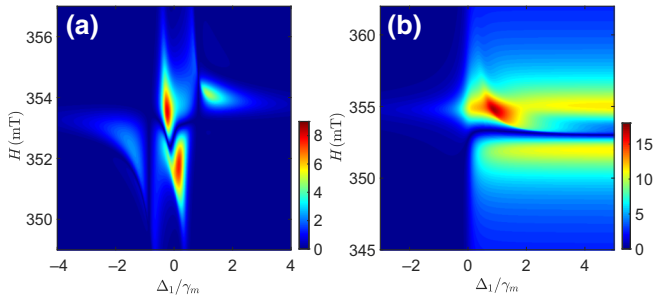


FIG. 5. The calculation results for  $I$  (in decibels) versus  $\Delta_1/\gamma_m$  and the external magnetic field  $H$ : (a)  $J = 0.5\gamma_m$ ,  $P_3 = 0$  mW, and  $P_1 = P_2 = 200$  mW; (b)  $J = \sqrt{(\Delta_1^2 + \kappa_1^2)/4}/3$ ,  $P_3 = 10$  mW, and  $P_1 = P_2 = 100$  mW.  $\Delta_2 = \Delta_1$ , and the other parameters are the same as in Fig. 2.

$\Delta_1/\gamma_m$  for obtaining nonreciprocal transmission immediately becomes larger and, what is more, the nonreciprocal isolation ratio is also improved, although this not very obvious. When the input power  $P_3$  increases to 10 mW [see the black dotted curve], it can be seen that the amplitude of  $I$  gains a further increase compared to the case for  $P_3 = 1$  mW. It is worth mentioning that the maximal value of  $I$  for the black dotted curve becomes 17.3 dB from 6.1 dB for the blue dotted curve near  $\Delta_1/\gamma_m = 0.9$ . This is the result of a stronger response of the magnon Kerr nonlinearity due to the effect of the strengthening of the driving field on the magnon mode. If a continue to enhance the input power  $P_3$ , we observe an analogous evolutionary trend for  $I$ , with its peak value reaching 21 dB [see the red curve], which is actually an extremely high nonreciprocal isolation ratio ( $> 20$  dB) [56]. Moreover, owing to magnon Kerr nonlinearity, this change in the magnonic response then modifies the resonance frequency of the hybridization of the two cavity photons and the magnons, which is embodied in the shift of the detuning  $\Delta_1/\gamma_m$  corresponding to the peak value of  $I$ .

#### IV. CONCLUSIONS

In summary, magnon-induced nonreciprocal transmission via magnon Kerr nonlinearity is shown in a two-cavity magnonics system. We demonstrate that the different magnonic responses are enabled by tuning the coupling strength  $J$  between the two microwave cavities, which causes the impedance-matching condition to break, or by taking advantage of an additional microwave source driving the magnon mode. It is found that the magnonic responses not only need to be different but also strong enough to produce nonreciprocal transmission via the breaking of the Lorentz reciprocity based on the magnon Kerr effect. Two kinds of cases, including the destruction of the impedance-matching condition and an additional driving field applied to the magnon mode to observe the

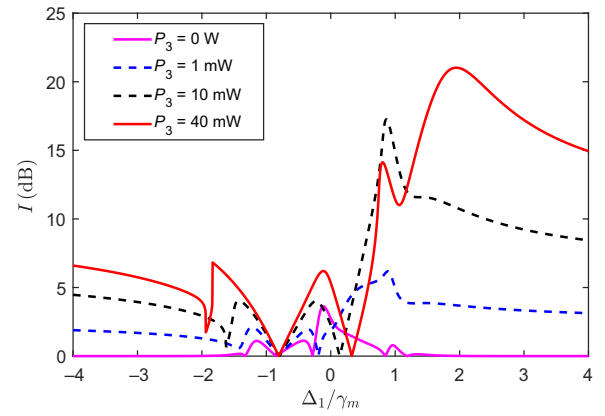


FIG. 6. The efficiency  $I$  for the nonreciprocal transmission of a microwave field as a function of the detuning  $\Delta_1/\gamma_m$ . We set  $J = 0.5\gamma_m$ ,  $P_1 = P_2 = 100$  mW, and  $\Delta_m = \Delta_2 = \Delta_1$ , and the other parameters are the same as in Fig. 2.

nonreciprocal transmission of the microwave field, are verified by the numerical simulation. In addition, we exhibit magnetically tunable nonreciprocal transmission by making use of the intrinsically good flexibility of the frequency of the magnon, determined by the external bias magnetic field. By enhancing the strength of the microwave source driving the magnon mode, a robust nonreciprocal isolation ratio can be obtained, which is easily implemented in practice. These exotic features of the two-cavity magnonics system greatly widen the perspectives for exploring the nonlinearity of magnons on the basis of the magnon Kerr effect. Nonreciprocal transmission is fundamental to the realization of efficient information processing and magnon-induced nonreciprocal transmission will be in great demand in microwave information processing, such as the design and achievement of magnetically controllable isolators and diodes.

#### ACKNOWLEDGMENTS

The work was supported by the National Key Research and Development Program of China (Grant No. 2016YFA0301203), the National Science Foundation of China (Grants No. 11774113 and No. 11875029), and the Fundamental Research Funds for the Central Universities (Grant No. 2019kfyRCPY111).

- [1] Ö. O. Soykal and M. E. Flatté, Strong Field Interactions Between a Nanomagnet and a Photonic Cavity, *Phys. Rev. Lett.* **104**, 077202 (2010).
- [2] X.-F. Zhang, C.-L. Zou, L. Jiang, and H. X. Tang, Strongly Coupled Magnons and Cavity Microwave Photons, *Phys. Rev. Lett.* **113**, 156401 (2014).
- [3] L. H. Bai, M. Harder, Y. P. Chen, X. Fan, J. Q. Xiao, and C.-M. Hu, Spin Pumping in Electrodynamically Coupled

- Magnon-Photon Systems, *Phys. Rev. Lett.* **114**, 227201 (2015).
- [4] J. Bourhill, N. Kostylev, M. Goryachev, D. L. Creedon, and M. E. Tobar, Ultrahigh cooperativity interactions between magnons and resonant photons in a YIG sphere, *Phys. Rev. B* **93**, 144420 (2016).
- [5] N. Kostylev, M. Goryachev, and M. E. Tobar, Superstrong coupling of a microwave cavity to yttrium iron garnet magnons, *Appl. Phys. Lett.* **108**, 062402 (2016).
- [6] C. Kong, B. Wang, Z.-X. Liu, H. Xiong, and Y. Wu, Magnetically controllable slow light based on magnetostrictive forces, *Opt. Express* **27**, 5544 (2019).
- [7] Y. Tabuchi, S. Ishino, T. Ishikawa, R. Yamazaki, K. Usami, and Y. Nakamura, Hybridizing Ferromagnetic Magnons and Microwave Photons in the Quantum Limit, *Phys. Rev. Lett.* **113**, 083603 (2014).
- [8] H. Huebl, C. W. Zollitsch, J. Lotze, F. Hocke, M. Greifenstein, A. Marx, R. Gross, and S. T. B. Goennenwein, High Cooperativity in Coupled Microwave Resonator Ferromagnetic Insulator Hybrids, *Phys. Rev. Lett.* **111**, 127003 (2013).
- [9] M. Goryachev, W. G. Farr, D. L. Creedon, Y. Fan, M. Kostylev, and M. E. Tobar, High-cooperativity Cavity QED with Magnons at Microwave Frequencies, *Phys. Rev. Appl.* **2**, 054002 (2014).
- [10] D. Zhang, X. M. Wang, T. F. Li, X. Q. Luo, W. Wu, F. Nori, and J. Q. You, Cavity quantum electrodynamics with ferromagnetic magnons in a small yttrium-iron-garnet sphere, *npj Quantum Inf.* **1**, 15014 (2015).
- [11] V. Cherepanov, I. Kolokolov, and V. L'vov, The saga of YIG: Spectra, thermodynamics, interaction and relaxation of magnons in a complex magnons, *Phys. Rep.* **229**, 81 (1993).
- [12] W. G. Farr, M. Goryachev, D. L. Creedon, and M. E. Tobar, Strong coupling between whispering gallery modes and chromium ions in ruby, *Phys. Rev. B* **90**, 054409 (2014).
- [13] M. Goryachev, W. G. Farr, D. L. Creedon, and M. E. Tobar, Spin-photon interaction in a cavity with time-reversal symmetry breaking, *Phys. Rev. B* **89**, 224407 (2014).
- [14] K. Benmessai, M. E. Tobar, N. Bazin, P.-Y. Bourgeois, Y. Kersalé, and V. Giordano, Creating traveling waves from standing waves from the gyrotropic paramagnetic properties of  $\text{Fe}^{3+}$  ions in a high- $Q$  whispering gallery mode sapphire resonator, *Phys. Rev. B* **79**, 174432 (2009).
- [15] M. W. Doherty, F. Dolde, H. Fedder, F. Jelezko, J. Wrachtrup, N. B. Manson, and L. C. L. Hollenberg, Theory of the ground-state spin of the  $\text{NV}^-$  center in diamond, *Phys. Rev. B* **85**, 205203 (2012).
- [16] Y. Tabuchi, S. Ishino, A. Noguchi, T. Ishikawa, R. Yamazaki, K. Usami, and Y. Nakamura, Coherent coupling between a ferromagnetic magnon and a superconducting qubit, *Science* **349**, 405 (2015).
- [17] D. Lachance-Quirion, Y. Tabuchi, S. Ishino, A. Noguchi, T. Ishikawa, R. Yamazaki, and Y. Nakamura, Resolving quanta of collective spin excitations in a millimeter-sized ferromagnet, *Sci. Adv.* **3**, e1603150 (2017).
- [18] X.-F. Zhang, C.-L. Zou, L. Jiang, and H. X. Tang, Cavity magnomechanics, *Sci. Adv.* **2**, e1501286 (2016).
- [19] X.-F. Zhang, N. Zhu, C.-L. Zou, and H. X. Tang, Optomagnonic Whispering Gallery Microresonators, *Phys. Rev. Lett.* **117**, 123605 (2016).
- [20] A. Osada, R. Hisatomi, A. Noguchi, Y. Tabuchi, R. Yamazaki, K. Usami, M. Sadgrove, R. Yalla, M. Nomura, and Y. Nakamura, Cavity Optomagnonics with Spin-Orbit Coupled Photons, *Phys. Rev. Lett.* **116**, 223601 (2016).
- [21] S. Sharma, Y. M. Blanter, and G. E. W. Bauer, Optical Cooling of Magnons, *Phys. Rev. Lett.* **121**, 087205 (2018).
- [22] M. Aspelmeyer, T. J. Kippenberg, and F. Marquardt, Cavity optomechanics, *Rev. Mod. Phys.* **86**, 1391 (2014).
- [23] B. Wang, Z.-X. Liu, C. Kong, H. Xiong, and Y. Wu, Magnon induced transparency and amplification in PT-symmetric cavity magnon system, *Opt. Express* **26**, 20248 (2018).
- [24] M. Harder, L. Bai, P. Hyde, and C. M. Hu, Topological properties of a coupled spin-photon system induced by damping, *Phys. Rev. B* **95**, 214411 (2017).
- [25] D. Zhang, X.-Q. Luo, Y.-P. Wang, T.-F. Li, and J. Q. You, Observation of the exceptional point in cavity magnon-polaritons, *Nat. Commun.* **8**, 1368 (2017).
- [26] G.-Q. Zhang and J. Q. You, Higher-order exceptional point in a cavity magnonics system, *Phys. Rev. B* **99**, 054404 (2019).
- [27] X.-F. Zhang, C.-L. Zou, N. Zhu, F. Marquardt, L. Jiang, and H. X. Tang, Magnon dark modes and gradient memory, *Nat. Commun.* **6**, 8914 (2015).
- [28] A. V. Chumak, V. I. Vasyuchka, A. A. Serga, and B. Hillebrands, Magnon spintronics, *Nat. Phys.* **11**, 453 (2015).
- [29] K. Uchida, J. Xiao, H. Adachi, J. Ohe, S. Takahashi, J. Ieda, T. Ota, Y. Kajiwara, H. Umezawa, H. Kawai, G. E. W. Bauer, S. Maekawa, and E. Saitoh, Spin Seebeck insulator, *Nat. Mater.* **9**, 894 (2010).
- [30] L. Bai, M. Harder, P. Hyde, Z. Zhang, C. M. Hu, Y. P. Chen, and J. Q. Xiao, Cavity Mediated Manipulation of Distant Spin Currents Using a Cavity-Magnon-Polariton, *Phys. Rev. Lett.* **118**, 217201 (2017).
- [31] B. Yao, Y. S. Gui, J. W. Rao, S. Kaur, X. S. Chen, W. Lu, Y. Xiao, H. Guo, K. P. Marzlin, and C. M. Hu, Cooperative polariton dynamics in feedback-coupled cavities, *Nat. Commun.* **8**, 1437 (2017).
- [32] G. Q. Zhang, Y. P. Wang, and J. Q. You, Theory of the magnon Kerr effect in cavity magnonics, *Sci. China-Phys. Mech. Astron.* **62**, 987511 (2019).
- [33] Y.-P. Wang, G.-Q. Zhang, D. Zhang, X.-Q. Luo, W. Xiong, S.-P. Wang, T.-F. Li, C.-M. Hu, and J. Q. You, Magnon Kerr effect in a strongly coupled cavity-magnon system, *Phys. Rev. B* **94**, 224410 (2016).
- [34] Y.-P. Wang, G. Q. Zhang, D. Zhang, T. F. Li, C. M. Hu, and J. Q. You, Bistability of Cavity Magnon-Polaritons, *Phys. Rev. Lett.* **120**, 057202 (2018).
- [35] Z.-X. Liu, B. Wang, H. Xiong, and Y. Wu, Magnon-induced high-order sideband generation, *Opt. Lett.* **43**, 3698 (2018).
- [36] M. Hafezi and P. Rabl, Optomechanically induced non-reciprocity in microring resonators, *Opt. Express* **20**, 7 (2012).
- [37] Z. Shen, Y.-L. Zhang, Y. Chen, C.-L. Zou, Y.-F. Xiao, X.-B. Zou, F.-W. Sun, G.-C. Guo, and C.-H. Dong, Experimental realization of optomechanically induced non-reciprocity, *Nat. Photon.* **10**, 657 (2016).
- [38] M. Terraneo, M. Peyrard, and G. Casati, Controlling the Energy Flow in Nonlinear Lattices: A Model for a Thermal Rectifier, *Phys. Rev. Lett.* **88**, 094302 (2002).



- [39] L. Fan, J. Wang, L. T. Varghese, H. Shen, B. Niu, Y. Xuan, A. M. Weiner, and M. Qi, An all-silicon passive optical diode, *Science* **335**, 447 (2012).
- [40] B. Liang, B. Yuan, and J.-C. Cheng, Acoustic Diode: Rectification of Acoustic Energy Flux in One-Dimensional Systems, *Phys. Rev. Lett.* **103**, 104301 (2009).
- [41] V. V. Konotop and V. Kuzmiak, Nonreciprocal frequency doubler of electromagnetic waves based on a photonic crystal, *Phys. Rev. B* **66**, 235208 (2002).
- [42] E. Verhagen and A. Alù, Optomechanical nonreciprocity, *Nat. Phys.* **13**, 922 (2017).
- [43] D. L. Sounas and A. Alù, Non-reciprocal photonics based on time modulation, *Nat. Photon.* **11**, 774 (2017).
- [44] R. J. Potton, Reciprocity in optics, *Rep. Prog. Phys.* **67**, 717 (2004).
- [45] F. D. M. Haldane and S. Raghu, Possible Realization of Directional Optical Waveguides in Photonic Crystals with Broken Time-Reversal Symmetry, *Phys. Rev. Lett.* **100**, 013904 (2008).
- [46] Y. Hadad and B. Z. Steinberg, Magnetized Spiral Chains of Plasmonic Ellipsoids for One-Way Optical Waveguides, *Phys. Rev. Lett.* **105**, 233904 (2010).
- [47] D. Malz, L. D. Tóth, N. R. Bernier, A. K. Feofanov, T. J. Kippenberg, and A. Nunnenkamp, Quantum-Limited Directional Amplifiers with Optomechanics, *Phys. Rev. Lett.* **120**, 023601 (2018).
- [48] Z. Shen, Y.-L. Zhang, Y. Chen, F.-W. Sun, X.-B. Zou, G.-C. Guo, C.-L. Zou, and C.-H. Dong, Reconfigurable optomechanical circulator and directional amplifier, *Nat. Commun.* **9**, 1797 (2018).
- [49] S. Barzanjeh, M. Wulf, M. Peruzzo, M. Kalaei, P. B. Dieterle, O. Painter, and J. M. Fink, Mechanical on-chip microwave circulator, *Nat. Commun.* **8**, 953 (2017).
- [50] A. A. Serga, A. V. Chumak, and B. Hillebrands, YIG magnonics, *J. Phys. D Appl. Phys.* **43**, 264002 (2010).
- [51] B. Lenk, H. Ulrichs, F. Garbs, and M. Münzenberg, The building blocks of magnonics, *Phys. Rep.* **507**, 107 (2011).
- [52] H. Xiong and Y. Wu, Fundamentals and applications of optomechanically induced transparency, *Appl. Phys. Rev.* **5**, 031305 (2018).
- [53] Z.-X. Liu, H. Xiong, and Y. Wu, Room-temperature slow light in a coupled cavity magnon-photon system, *IEEE Access* **7**, 57047 (2019).
- [54] T. Shui, W.-X. Yang, L. Li, and X. Wang, Lop-sided Raman-Nath diffraction in PT-antisymmetric atomic lattices, *Opt. Lett.* **44**, 2089 (2019).
- [55] X.-W. Xu, L. N. Song, Q. Zheng, Z. H. Wang, and Y. Li, Optomechanically induced nonreciprocity in a three-mode optomechanical system, *Phys. Rev. A* **98**, 063845 (2018).
- [56] S. Manipatruni, J. T. Robinson, and M. Lipson, Optical Nonreciprocity in Optomechanical Structures, *Phys. Rev. Lett.* **102**, 213903 (2009).
- [57] T. Brecht, W. Pfaff, C. Wang, Y. Chu, L. Frunzio, M. H. Devoret, and R. J. Schoelkopf, Multilayer microwave integrated quantum circuits for scalable quantum computing, *npj Quantum Inf.* **2**, 16002 (2016).
- [58] C. W. Gardiner and P. Zoller, *Quantum Noise* (Springer, New York, 2004).